Nanoscopic cell-wall architecture of an immunogenic ligand in *Candida albicans* during antifungal drug treatment

Jia Lin[a,b], Michael J. Wester[a,c], Matthew S. Graus[a,b], Keith A. Lidke[a,d], and Aaron K. Neumann[a,b,*]
[a]Center for Spatiotemporal Modeling of Cell Signaling, [b]Department of Pathology, [c]Department of Mathematics and Statistics, and [d]Department of Physics and Astronomy, University of New Mexico, Albuquerque, NM 87131

ABSTRACT **The cell wall of *Candida albicans* is composed largely of polysaccharides. Here we focus on β-glucan, an immunogenic cell-wall polysaccharide whose surface exposure is often restricted, or "masked," from immune recognition by Dectin-1 on dendritic cells (DCs) and other innate immune cells. Previous research suggested that the physical presentation geometry of β-glucan might determine whether it can be recognized by Dectin-1. We used direct stochastic optical reconstruction microscopy to explore the fine structure of β-glucan exposed on *C. albicans* cell walls before and after treatment with the antimycotic drug caspofungin, which alters glucan exposure. Most surface-accessible glucan on *C. albicans* yeast and hyphae is limited to isolated Dectin-1–binding sites. Caspofungin-induced unmasking caused approximately fourfold to sevenfold increase in total glucan exposure, accompanied by increased phagocytosis efficiency of DCs for unmasked yeasts. Nanoscopic imaging of caspofungin-unmasked *C. albicans* cell walls revealed that the increase in glucan exposure is due to increased density of glucan exposures and increased multiglucan exposure sizes. These findings reveal that glucan exhibits significant nanostructure, which is a previously unknown physical component of the host–*Candida* interaction that might change during antifungal chemotherapy and affect innate immune activation.**

Monitoring Editor
Jennifer Lippincott-Schwartz
National Institutes of Health

Received: Jun 10, 2015
Revised: Dec 12, 2015
Accepted: Jan 12, 2016

INTRODUCTION

Candida albicans is a normal commensal fungus living on various human mucosal surfaces and also an opportunistic pathogen that can cause superficial or systemic infections. Healthcare costs associated with treatment of candidiasis exceed $1 billion annually in the United States alone (Wenzel and Edmond, 2001; Anderson *et al.*, 2007). *C. albicans* is a dimorphic fungus that can exist as yeast or transition to invasive growth as filamentous hyphal cells under infection-relevant conditions, and these hyphae are able to penetrate epithelial and endothelial tissues (Davies *et al.*, 1999). Switching of *C. albicans* between the two morphological forms is believed to be crucial to pathogenesis of invasive candidiasis because *C. albicans* locked in either yeast or hyphal forms is hypovirulent (Lo *et al.*, 1997; Murad *et al.*, 2001; Grubb *et al.*, 2008; Cheng *et al.*, 2012).

The fungal cell-wall surface provides the protein and carbohydrate ligands that establish and maintain contact with host cells of the innate immune and mucocutaneous systems. The *Candida* cell wall contains the polysaccharides chitin, β-(1,3:1,6)-D-glucan, and N- and O-linked mannans. Dendritic cells (DCs) and other leukocytes sense fungal cell-wall polysaccharides via pattern recognition receptors (PRRs) such as the transmembrane C-type lectins (CTLs) DC-SIGN and Dectin-1, which bind mannan and β-(1,3)-D-glucan, respectively. Recognition of β-glucan by Dectin-1 provides powerful immunogenic signals capable of driving fungal phagocytosis and cellular activation in innate immune cells (Brown *et al.*, 2002, 2003; Rogers *et al.*, 2005). When activated via PRRs, DCs fulfill critical roles in innate and adaptive immunity as sentinels of pathogen entry and antigen-presenting cells for stimulating T-lymphocytes (Banchereau and Steinman, 1998). Therefore regulation of the amount and exposure of immunogenic cell-wall ligands is an important facet of the host–pathogen interaction that is the subject of active investigation.

This article was published online ahead of print in MBoC in Press (http://www.molbiolcell.org/cgi/doi/10.1091/mbc.E15-06-0355) on January 20, 2016.
*Address correspondence to: Aaron K. Neumann (akneumann@salud.unm.edu).
Abbreviation used: dSTORM, direct stochastic optical reconstruction microscopy.

Whereas mannan is abundantly exposed at the surface of *C. albicans* cell walls, studies have shown that β-glucan exhibits a much more limited, punctate exposure in resting *C. albicans* yeasts (Gantner *et al.*, 2005). However, conditions such as treatment with the antimycotic drug caspofungin, hyphal germination, and neutrophilic attack have been reported to cause a phenotype of increased β-glucan exposure in *C. albicans* cell walls as observed by conventional, diffraction-limited imaging and other methods (Wheeler and Fink, 2006; Wheeler *et al.*, 2008). These observations led to the influential concept that *C. albicans* suppresses its immunogenicity by "masking" cell-wall β-glucan and that increases in β-glucan exposure resulting from damage to or structural alteration of the *C. albicans* cell wall increase immunogenicity of the fungal particle. Caspofungin is the first of the echinocandin class of antifungal drugs that is used to treat fungal infections. This drug inhibits Fks1p to abrogate cell-wall synthesis of β-(1,3)-D-glucan, destabilizing the cell wall, increasing the exposure of β-glucan (Figure 1), and increasing leukocyte responses relative to untreated fungi (Keating and Figgitt, 2003; Mccormack *et al.*, 2005; Wheeler and Fink, 2006; Wheeler *et al.*, 2008; Lamaris *et al.*, 2008; Bizerra *et al.*, 2011; El-Kirat-Chatel *et al.*, 2013). The fine-scale structural changes to β-glucan exposure geometry during masking/unmasking processes remain obscure and require further characterization using methods capable of nanoscopic resolution.

Dectin-1 binds soluble β-glucan, as well as purified particulate β-glucan, a form of the ligand more likely to resemble β-glucan present in the cell wall (Brown *et al.*, 2007; Adams *et al.*, 2008). DCs produce a reactive oxygen species (ROS) burst in response to glucan-coated beads of 500-nm diameter but not for 200-nm or smaller glucan particles, suggesting that glucan sensing may depend on physical characteristics of glucan presentation at nanometric dimensions (Goodridge *et al.*, 2011). However, the specific nanoscale dimension of β-glucan exposure that is relevant to Dectin-1 activation remains unclear. The exact size of the contact site between the beads and leukocytes is unknown, but it is likely to be considerably smaller than the bead diameter and depend on factors such as radius of curvature of the bead, strength of receptor/ligand binding interactions, local membrane composition, and membrane bending energy. The ligand size dependence of Dectin-1 signaling suggests that masked β-glucan exposures could be predominantly restricted to some nonstimulatory sizes, whereas unmasking processes could create larger exposures of β-glucan capable of better stimulating Dectin-1. The resolution of conventional optical microscopy (~300 nm under ideal conditions) is insufficient to directly observe these hypothetical changes in *C. albicans* cell-wall β-glucan exposure.

Direct stochastic optical reconstruction microscopy (dSTORM) is a form of localization microscopy that achieves superresolution imaging (~20-nm precision) of biological structures labeled by means of organic dye–conjugated affinity probes. dSTORM builds up an image from many sequential ~20 nm–precision localizations of individual dyes in the specimen (van de Linde *et al.*, 2011). Given the goals of analysis and nature of the data, various useful methods are available to assess β-glucan nanostructure in dSTORM data sets. Measurements such as Ripley's *K* statistic and pair autocorrelation quantify spatial nonrandomness (e.g., clustering) as a function of length scale (Jain and Dubes, 1988; Zhang *et al.*, 2006; Sengupta *et al.*, 2013). These methods both operate on ensembles of individual structures within each imaging region of interest and return an overall quantification of structure. Cluster detection methods, such as density-based spatial clustering of applications with noise (DBSCAN), a modified Getis–Ord *G* spatial statistic, Ripley's *K*

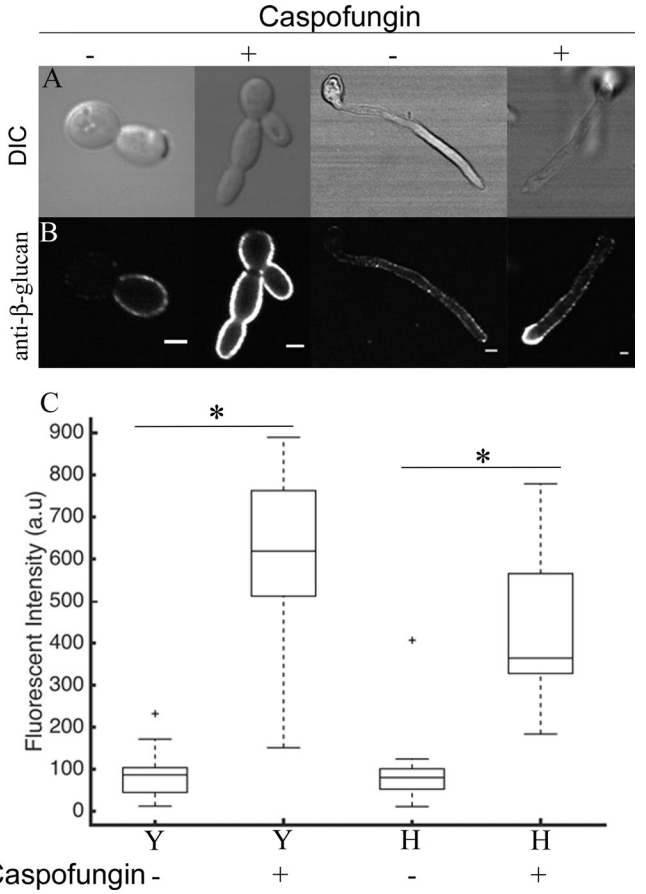

FIGURE 1: Caspofungin treatment increases in total β-glucan exposure on *C. albicans* cell walls. (A, B) Bright-field (A) and confocal fluorescence (B) images of yeast (Y) and hyphae (H), with (+) and without (–) caspofungin treatment. Scale bar, 2 μm. (C) Box plots depicting the median background-subtracted fluorescence intensity (solid line inside box) of β-glucan staining observed under all conditions. The median intensity values are Y–, 86; Y+, 618; H–, and 80; H+, 364. The boxes represent the IQR (25th to 75th percentile of the data set). The whiskers represent 1–99% of the data. The outliers (+) represent data points outside of these limits. Statistical comparisons were performed using the Mann–Whitney *U* test (*$p < 0.01$). These data represent comparisons of intensity distributions from $N_{min} = 25$ yeasts/group.

thresholding, topographical prominence, hierarchical clustering, and Voronoï tessellation–based segmentation are options for objectively defining glucan exposures for further characterization (Ord and Getis, 1995; Ester *et al.*, 1996; Itano *et al.*, 2014; Griffié *et al.*, 2015; Levet *et al.*, 2015; Rubin-Delanchy *et al.*, 2015). In general, these clustering methods operate by detecting local increases in dSTORM localization density, potentially allowing subpopulations of objects with different structural features to be examined. These clustering methods do not address a common issue in dSTORM imaging—multiple localizations in the data set representing single probes on the specimen. In our work, we sought to provide suitable estimates of single probe positions in the presence of multiple dSTORM localization artifacts using novel methods and performed clustering analysis with the robust DBSCAN algorithm.

In the present work, we spatially characterize β-glucan exposures in the *C. albicans* cell wall with ~20-nm localization precision and test the hypothesis that cell-wall structural change results in an increase in the nanoscale dimension of β-glucan exposures.

RESULTS

Caspofungin causes higher β-glucan exposure on cell walls

To demonstrate consistency with previously reported experimental systems and quantify the increase in β-glucan exposure after caspofungin treatment, samples of *C. albicans* yeast and hyphae were prepared, treated with a subinhibitory dose of caspofungin, and stained for β-glucan exposure using anti–β-glucan antibody as described in *Materials and Methods*. Representative confocal fluorescence images of yeast and hyphae demonstrate the increase in β-glucan exposure observed after caspofungin treatment (Figure 1, A and B). We noted that hyphal tips often displayed greater glucan exposure than the lateral cell walls, and this phenotype was particularly pronounced in caspofungin-treated hyphae. We quantitatively compared β-glucan exposure in yeast and hyphae that were untreated or treated with caspofungin. The background-subtracted average fluorescence intensity of β-glucan probe over the surface of the fungal cell was quantified, and the distribution of β-glucan exposure intensities over at least 25 individual yeasts or hyphae was calculated (Figure 1C). Caspofungin unmasked β-glucan on cell walls of both yeast and hyphae, resulting in significantly greater anti–β-glucan staining in both cases. The magnitude of drug-induced β-glucan unmasking was 7.2-fold for yeast and overall 4.6-fold for hyphae.

β-Glucan unmasking increases phagocytosis

The greater glucan exposure of caspofungin-treated yeasts should lead primary human dendritic cells to engulf them more efficiently than untreated controls. The percentage of DCs having internalized one or more yeast(s) was ~46% of the total population for untreated yeast and 76% for treated yeast (Figure 2A). Furthermore, the mean DC phagocytic index was higher for caspofungin-treated yeast than for untreated yeast, meaning that individual DCs were able to more efficiently internalize yeasts after caspofungin-mediated unmasking (Figure 2B). These results are consistent with previous findings showing increased immunogenicity of *Candida* after unmasking (Wheeler and Fink, 2006).

dSTORM imaging of *C. albicans*

Previous work suggested that the nanoscale presentation geometry of glucan might be a significant determinant of DC activation during fungal recognition. However, the ~300-nm resolution limit of conventional optical imaging methods precluded direct measurements of the fine structure of β-glucan exposure. Therefore we used dSTORM imaging, which allows unprecedented optical resolution of β-glucan exposure geometries in the *C. albicans* cell wall. Quantitative description and comparison of β-glucan exposure geometries require spatial statistical tools to detect and measure clustering of localizations in dSTORM data sets. We therefore used several analytical approaches to quantify β-glucan nanostructure in dSTORM data sets of yeasts and hyphae with and without caspofungin treatment. However, before acquiring and analyzing nanoscopic β-glucan exposure data, we performed simulation studies to establish the optimal approach to imaging fungal cell-wall structure.

When a curved surface is imaged in two dimensions, projection distortion is possible. We optimized our approach to minimize nanostructure distortion and performed simulations to determine maximum expected projection distortion with our imaging approach. Total internal reflection fluorescence (TIRF) imaging is often used for cellular dSTORM to obtain a thin optical section, suppress background, and increase localization precision. However, due to the relatively high radius of curvature of fungal cell walls, TIRF imaging was not optimal for our specimens. Instead, we fixed and labeled *C. albicans* with Alexa Fluor 647–conjugated soluble Dectin-1, imaged coverglass-adhered fungi under standard dSTORM imaging conditions using oblique illumination, and collected data from an imaging plane located at $\phi = 60–90°$ of the yeast cell wall (Figure 3A). To investigate the imaging environment in this configuration, we implemented a simulation of hemispherical cell wall surface ($r_{curvature}$ = 2500 nm) covered with Gaussian-distributed domains (uniform σ = 22 nm) representing β-glucan exposures. To simulate the imaging process, domains on the curved surface were projected onto the equatorial plane over 10° arcs of ϕ (latitude), from ϕ = 90 (top of cell) to 0° (equator). We measured size distributions of domains (equivalent circular diameter) in projected images based on observed domain convex hull boundaries. The degree of distortion was measured as the ratio of the observed equivalent circular diameter to the input Gaussian diameter (2σ), so ratio = 1 represents no distortion, and smaller ratios indicate greater distortion. We observed progressively decreasing ratios approaching the equator of the cell, such that observed domains were only ~30% of the nominal size near the equator (Figure 3B). However, domains in the range of ϕ = 60–90°, which approximate the portion of cell wall imaged in our dSTORM experiments, were subject to little distortion (ratio ≥ 0.9). We concluded that domains measured in our dSTORM images taken from the tops of yeasts and hyphae would be expected to contain very little projection distortion, which would result in no more than a 10% reduction in the measured domain diameter relative to the true value.

Representative examples of dSTORM data sets are shown in Figure 4. dSTORM

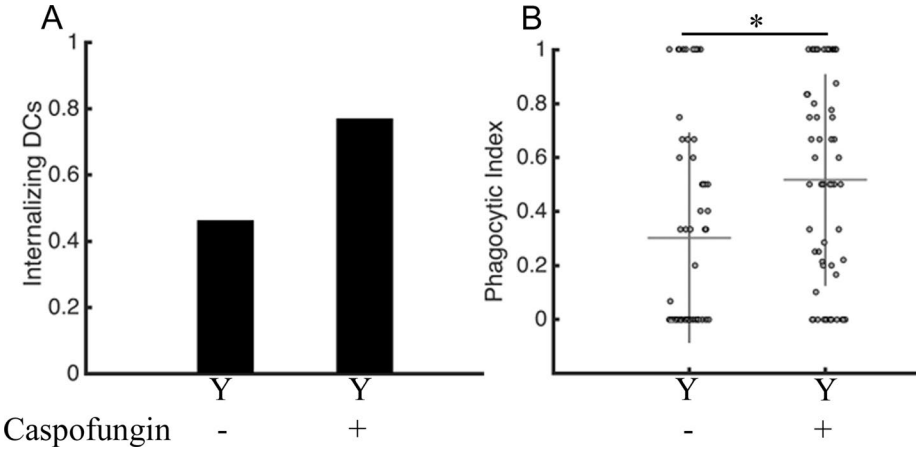

FIGURE 2: Caspofungin-induced β-glucan unmasking correlates with increased phagocytosis of *C. albicans* yeast. (A) The fraction of DCs having internalized ≥1 yeast after 1-h exposure to *C. albicans* was higher for caspofungin-treated yeast than with untreated controls. (B) Phagocytic index of DCs was significantly higher when challenged with caspofungin-treated *C. albicans* yeasts (○, individual DCs). Statistical comparisons were performed by the Mann–Whitney *U* test, and brackets indicate statistically significant differences (*$p < 0.05$). For all groups, N_{min} = 50 for each condition of total DCs analyzed. Data are aggregated from experiments using cells from two independent donors.

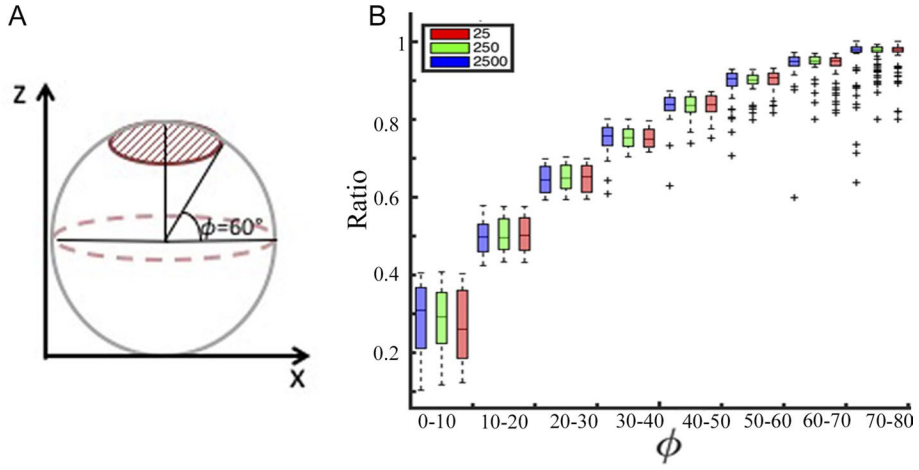

FIGURE 3: Distortion estimation and metrics for glucan exposures in superresolved micrographs. (A) Superresolution imaging of the curved cell-wall surface in a planar image could give rise to projection distortion that would affect the accuracy of glucan exposure geometry measurements. The circle represents a fungal cell wall in cross section for a spheroidal yeast or cylindrical hypha. To minimize both background from dyes nonspecifically adsorbed to glass (i.e., at $\phi = -90°$) and projection distortion, we performed dSTORM measurements by oblique illumination of the top of the labeled *C. albicans* cell and focused at the $\phi = 60–90°$ section of the cell, highlighted in red. (B) To place upper limits on geometric distortion effects, we simulated Gaussian-distributed domains ($s = 22$ nm) randomly distributed across a surface with radius of curvature similar to that of a *C. albicans* yeast ($r = 2500$ nm). After planar projection of all domains within 10° arcs from $\phi = 0$ to 90°, we calculated the ratio of identified cluster diameter (equivalent circular diameter of observed convex hull) vs. simulated cluster diameter ($2s$). Approaching $\phi = 90°$ (top of cell), this ratio is close to 1, indicating that distortion is negligible. Projection distortion is maximal at $\phi = 0°$ (side of cell), where domain diameters observed are only ~25–30% of the simulated size. In practice, our imaging depth of field from a focal plane at the top of the yeast provided a circular image of the radius, indicating that we were sampling structures from $\phi = 60$ to 90° on the *C. albicans* cell. Over this range, simulated diameter ratios do not fall below 90%, indicating that the effect of projection distortion on our measured domain sizes is anticipated to be minimal. The number of particles per domain, simulating individual dSTORM single-molecule localization events, was varied over three orders of magnitude (red, green, and blue bars), resulting in no effect on the foregoing conclusion.

localization positional fitting (single emitter) and β-glucan exposure analysis were done as per *Materials and Methods*. Exposure analysis was performed on user-selected 1 μm × 1 μm regions of interest (ROIs) that were chosen to minimize the curvature effect. One ROI was analyzed per cell over multiple cells imaged (minimum seven cells per condition).

Hierarchical single-emitter hypothesis test decreases the probe overcounting problem associated with dSTORM imaging

dSTORM produces pointillistic data sets of fluorophore coordinates. Owing to the stochastic nature of dye blinking during acquisition, individual probes may be represented by varying number of localizations within one dSTORM data set. Cluster analysis algorithms operating on raw dSTORM localization data might detect artificial structures due to apparent clustering arising from overcounting the probes. Therefore methods to correct for the multiple localization effect are necessary to accurately quantify β-glucan exposure geometry. We developed a top-down hierarchical clustering algorithm in MATLAB, which we termed the hierarchical single-emitter hypothesis test (H-SET), to collapse clusters of observations of blinking fluorophores into a single estimate of the true location of the fluorophore (Figure 5). Briefly, this method created a hierarchy of observations based on interpoint distances. Each node in the resulting dendrogram represented a set of points that is spatially associated at the specified distance. Starting with the most inclusive node, we applied a statistical hypothesis test to determine whether the set of observations was consistent with multiple localizations of a single emitter. If not, the algorithm moved to proximal nodes in the hierarchy to perform the same test on a shorter distance scale. This process was iterated until all observations in the data set were identified with a node that passed the statistical hypothesis test. For more details, see *Materials and Methods*).

We validated the ability of the H-SET to estimate emitter localizations in a simulated data set incorporating a realistic model of dSTORM multiple observations of probes. We simulated domains with a uniform random distribution in the simulation space and domain center separations ≥100 nm. The number of domains was based on the experimentally observed density of β-glucan exposures. Each domain was intended to simulate a single protein-based probe (i.e., AF647-conjugated rhDectin-1 ectodomain), which may have a small but variable number of dyes attached to it. About each simulated localization, we placed a Poisson-distributed number (mean = 3) of simulated observations, which were normally distributed in space according to a variable localization precision representative of the distribution of experimentally observed dSTORM localization precisions. These simulated observations represented individual dSTORM positional observations. Any observations outside the user-specified ROI size were eliminated. Examples of simulated data sets are shown in Figure 6, A and E. Here the red

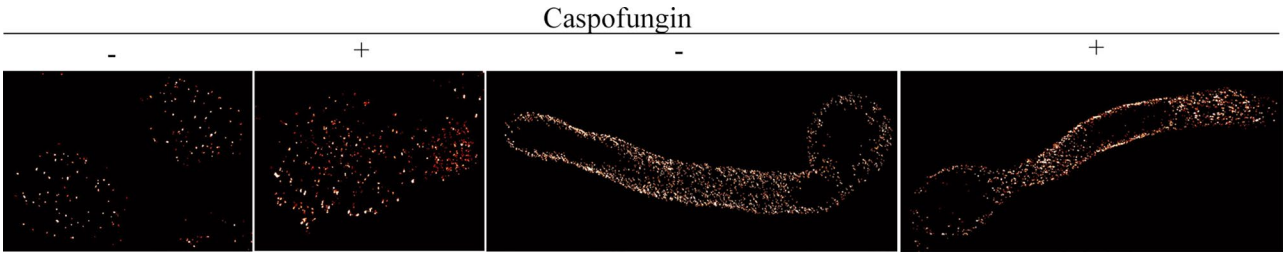

FIGURE 4: Representative dSTORM images of untreated and treated *C. albicans* yeasts (left) and hyphae (right). These images are provided for illustration only and are not all shown at the same scale.

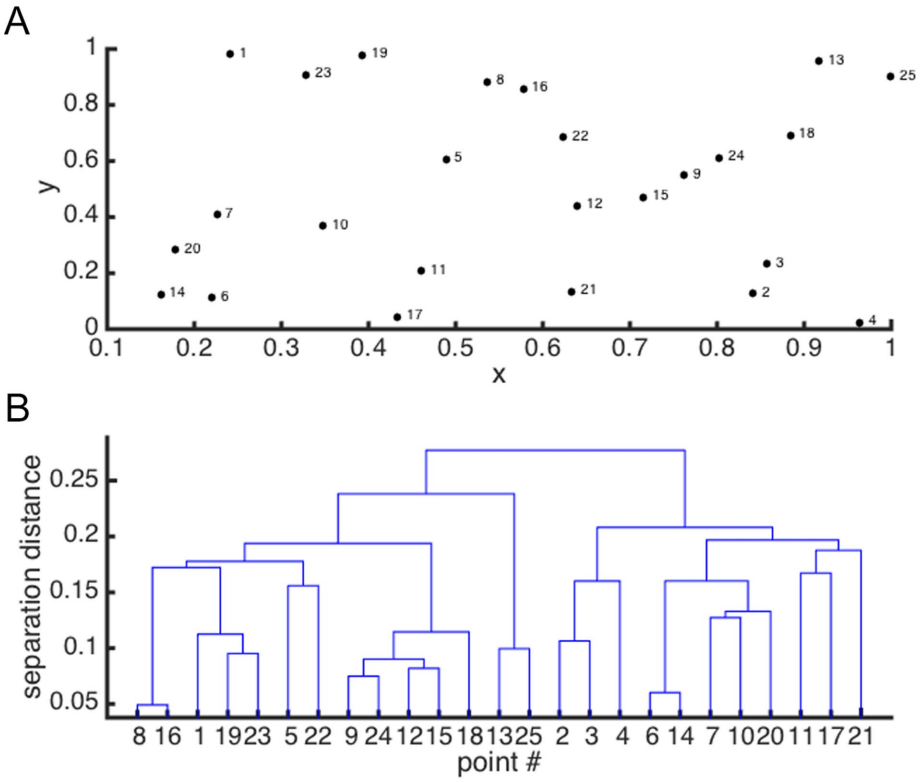

FIGURE 5: The top-down hierarchical single-emitter hypothesis test method. (A) A collection of observations (arbitrary positional units) and (B) the binary hierarchical linkage tree (MATLAB dendrogram plot) corresponding to them. The horizontal portions of the branches designate sets of observations that are connected at the distance indicated on the vertical axis.

dots represent the simulated localizations, the cyan dots are the simulated observations, and the blue dots are the recovered localizations derived by H-SET collapse of simulated multiple observations. Simulations were performed at a lower density (similar to that experimentally observed for untreated yeast) and a fivefold higher density (similar to experimental observations in drug-treated yeast). Further details regarding simulations are given in *Materials and Methods*.

The performance of H-SET was measured by comparing the number and position of recovered localizations to that of the simulated localizations. The distribution of the number of observations collapsed by H-SET into individual recovered localizations had a median of 3 (blue) in both simulated situations, whereas the input mean for simulation is 3 (red; Figure 6, B and F). In addition, the distribution of observations per recovered localization overlapped well with the distribution of input observations per simulated localization. Furthermore, we found that the number of recovered localizations agrees well with the number of simulated localizations (Figure 6, C and G). The median number of simulated localizations, recovered localizations, and observations was 38, 32, and 117, respectively, in the lower-density simulations (Figure 6C). For the higher-density simulations, the median number of simulated localizations, recovered localizations, and observations was 209, 175, and 630, respectively (Figure 6G). The mean distances between a recovered localization and the nearest simulated localization in the two simulated conditions were 8.6 and 8.7 nm, respectively (Figure 6, D and H), indicating that the positions of recovered localizations were in good agreement with simulated localizations. In attempting to recover single probe positions by H-SET, positional estimation errors are possible. Overcollapsing errors can occur where there is difficulty in distinguishing distributions of observations that are too close together. Undercollapsing errors may occur for individual dSTORM observations that had relatively low precision and might have been difficult to confidently group with other observations. However, we concluded that these errors were rare, and the H-SET provided overall reliable performance in collapsing multiple observations to allow accurate positional estimation of recovered localizations.

Altered β-glucan nanostructure after exposure to caspofungin

We hypothesized that drug-unmasked β-glucan exposures would increase in size, potentially driving some of them above a stimulatory size threshold. In addition, we note that increased density of total β-glucan exposures on the surface of the cell wall could be an additional mechanism to explain increasing glucan exposure upon unmasking. We treated *C. albicans* yeasts and hyphae with a subinhibitory dose of caspofungin (or no drug for controls). These specimens were fixed, labeled for β-glucan exposure, imaged by dSTORM, and compared with untreated controls using the foregoing spatial statistical analyses (Figures 5 and 6). Because these data sets contained multiple observations of individual probes, we further processed dSTORM data to estimate the positions of individual probes to minimize the effect of multiple counting on quantification of β-glucan exposures. First, our superresolution rendering approach used a frame connection method to combine data across multiple frames and calculate a single observation position, as long as the combined data met criteria for allowable separation in space and time (Smith *et al.*, 2010; Huang *et al.*, 2011). Second, we applied H-SET to dSTORM observations to collapse multiple localizations of a single probe into estimates of that probe's position. Furthermore, we used DBSCAN to objectively identify multiglucan exposures on cell walls, that is, exposure sites labeled by at least three probes in sufficiently close proximity to one another (see *Materials and Methods*). The boundary of multiglucan exposures was determined by the convex hull function in MATLAB. An example yeast dSTORM image analysis illustrates the spatial distribution of observations (cyan dots), localizations (blue dots), and DBSCAN identified multiglucan exposures (green lines; Figure 7A).

After application of H-SET to experimental dSTORM data sets, the median numbers of observations collapsed into a single localization were ~2 for Y– and H+, and 1 for Y+ and H–, respectively (Figure 7B), where Y = yeast, H = hypha, – = untreated, and + = caspofungin treated. This value was in good agreement with the number of observations collapsed per localization in dSTORM images of sparsely distributed AF647–Dectin-1 probe adsorbed to glass that were subjected to the same image analysis (Supplemental Figure S1). This indicates that H-SET is collapsing multiple dSTORM observations found in labeled cell walls as expected for identification of single probes. We quantified a statistically significant ~5.6-fold increase in total localization density (counts/square nanometer) for yeasts after caspofungin treatment (Figure 7C). The median glucan

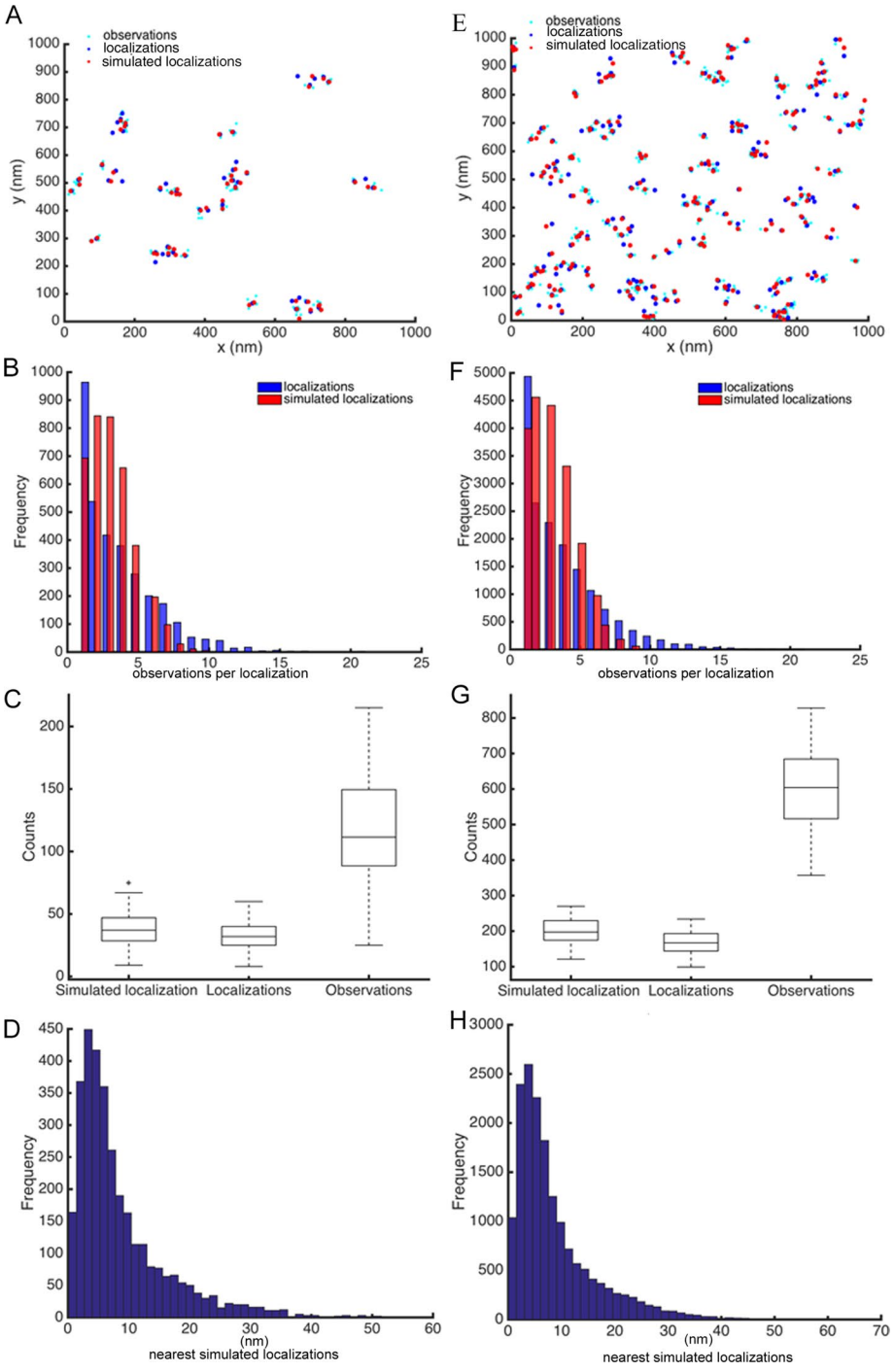

FIGURE 6: The hierarchical single-emitter hypothesis test method accurately corrects simulated dSTORM data sets for overcounting of multiply observed single emitters. Gaussian domains with a Poisson-distributed number of single emitters per domain were used to created distributions of simulated localizations. (A–D) Statistical analysis of simulated Gaussian domains with domain density of 10^{-5} domains/nm^2. (A) Sample image of color-coded locations of observations, localizations, and simulated localizations. (B) Histogram showing distributions of H-SET collapsed observations per localization (blue) with a median of three, and observations for simulated localization (red) with median of three. (C) The number of localizations is similar to the simulated localization, whereas the observations had much higher counts, as expected. (D) Histogram showing the distance from each recovered localization to the nearest simulated localization, which exhibited a mean distance of 8.6 nm. (E–H) Statistical analysis of simulated domains with domain density of 5×10^{-5} domains/nm^2. (F) Histogram showing a distribution of collapsed observations per localization (blue) with a median of three observations for simulated localization (red) and a median of three for the fivefold-higher domain density situation. (G) H-SET returned similar counts of simulated localizations and recovered localizations. (H) Histogram for higher domain density, showing the nearest distance of localizations to simulated localization with a mean distance of 8.7 nm. $N_{simulation}$ = 100/condition.

localization density for untreated yeast was 16 counts/nm^2, and we found 90 counts/nm^2 for treated yeasts. This value measures relative change in glucan exposure after drug treatment in dSTORM data sets, which we find to be similar to that observed by confocal microscopy (Figure 1). However, we did not observe a significant total dSTORM localization density change for untreated and treated hyphae (Figure 7C), despite having seen an increase in total glucan exposure in treated hyphae by confocal imaging (Figure 1). This discrepancy was likely due to technical difficulty with imaging hyphal tips by dSTORM (see *Discussion*). After classification of β-glucan exposures as singlet glucan or multiglucan exposures, we found that in all conditions, the large majority of glucan exposures were singlet glucan exposures (Figure 7D). We observed that hyphae exhibit a significantly smaller fraction of singlet glucan exposures relative to yeasts.

We observed significantly increased surface density of β-glucan exposure sites (including both singlet glucan and multiglucan exposures) after caspofungin treatment for yeasts relative to untreated yeasts (Figure 8A). The median nearest-neighbor distance between glucan exposure sites (considering singlet glucan and multiglucan exposures together) appeared to decrease in treated yeasts relative to untreated yeasts, but due to high variance in this parameter, it did not reach statistical significance (Supplemental Figure S2). Similarly, untreated hyphae had significantly greater β-glucan exposure-site surface density than untreated yeasts, but the lateral hyphal cell walls that we observed did not exhibit increased glucan exposure surface density after drug treatment. The medians of glucan exposure density (counts/nm^2) for the four conditions were Y–, 7×10^{-6}; Y+, 2.8×10^{-5}; H–, 3.3×10^{-5}; and H+, 3.2×10^{-5}. Because these measurements are inclusive of all glucan exposure sites (singlet glucan and multiglucan exposure), we also examined changes in density of singlet glucan and multiglucan exposure-site densities individually. We found that, in all cases in which glucan exposure was significantly increased, this difference was explained by an increase in both singlet glucan and multiglucan exposure-site densities (Supplemental Figure S3)

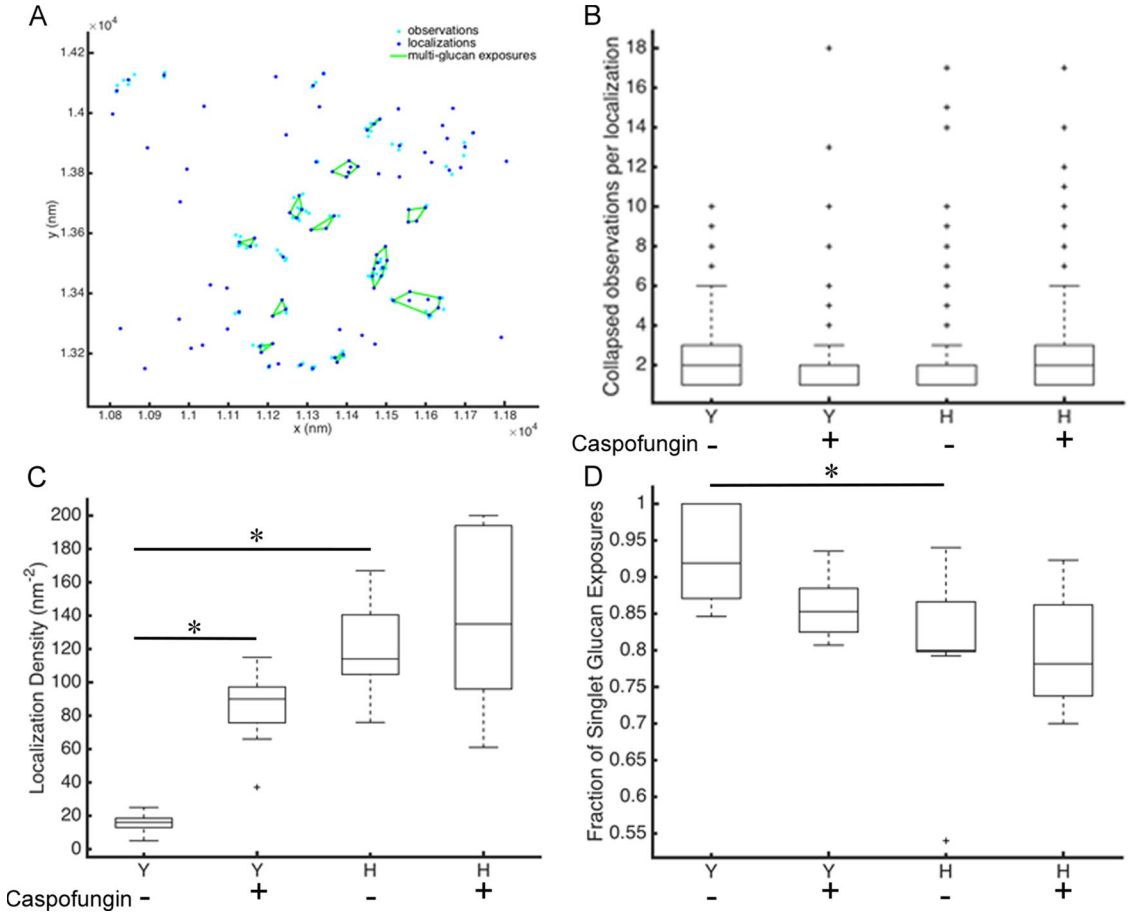

FIGURE 7: The hierarchical single-emitter hypothesis test reveals that the majority of glucan exposures are singlet glucan exposures on cell walls. Caspofungin treatment increases the number of Dectin-1–binding sites. (A) Sample yeast dSTORM data indicating the input dSTORM observations (cyan) and the localizations (blue) determined by the H-SET. Multiglucan exposures (green outlines) were identified using DBSCAN. (B) Median collapsed observations by the H-SET is ~2 for Y– and H+ and 1 for Y+ and H–. There are no significant differences among the conditions tested. (C) Drug treatment increases the density of localizations for yeast. There are significant differences in localization density between untreated and treated yeast and between untreated yeast and untreated hyphae. (D) Untreated hyphae exhibited a significantly lower fraction of singlet glucan exposures than do untreated yeast. However, singlet glucan exposures were the majority of exposures in all conditions tested, and drug treatment did not significantly change singlet glucan exposure for yeast or hyphae. *$p < 0.01$.

Because our analysis can classify glucan into singlet glucan and multiglucan exposures and measure these glucan nanostructures independently, we characterized the size of multiglucan exposures identified by DBSCAN. We observed that after caspofungin treatment, the size of multiglucan exposures increased. Median multiglucan exposure equivalent radius observed on the cell walls of treated yeast (19 nm) was significantly greater than that of untreated yeast (8.5 nm; Figure 8B). However, for hyphal lateral cell walls, we observed no change in multiglucan exposure size after drug treatment (22 nm for untreated, 26 nm after caspofungin; Figure 8B). Untreated hyphae did display significantly larger multiglucan exposures than untreated yeasts (Figure 8B). Furthermore, we quantified the number of unique dSTORM localizations per multiglucan exposure, which is an indicator of the multiplicity of Dectin-1/glucan binding sites within a multiglucan exposure. Figure 8C indicates that the median number of localizations per multiglucan exposure was, respectively, Y–, 3; Y+, 4; H–, 5; and H+, 5.6, respectively. Therefore drug-induced unmasking that resulted in larger multiglucan exposure structures did not cause a discernible increase in the internal count of receptor-binding sites within these structures. However, untreated hyphae did exhibit a modestly larger number of localizations per multiglucan exposure than untreated yeast cell walls.

Ripley's *K* function indicates overall randomness of β-glucan exposures

Having analyzed structure of glucan exposures at small length scales, we next used Ripley's *K* statistic to test for the existence of nonrandom organization of glucan exposures over longer length scales. In the absence of corrections for multiple localizations in dSTORM data, the dominant length scale of nonrandomness identified by Ripley's *K* statistic will correspond to multiple localizations of single dyes at the typical dSTORM precision of localization (~20 nm), but this provides no information about the true biological structure of glucan. Therefore we applied Ripley's *K* statistical analysis to dSTORM localizations obtained after H-SET (Figure 9). For each experimental dSTORM data set, we simulated a uniform random distribution of points with a point density matched to the mean localization density in the experimental data set. Experimental and simulated data were distributed in an equivalent 1 μm × 1 μm space,

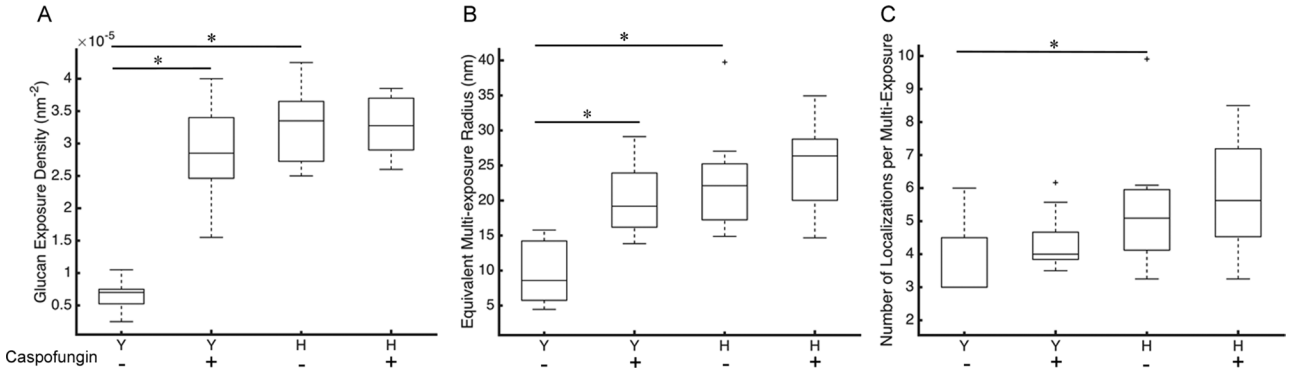

FIGURE 8: Caspofungin induces cell-wall remodeling, resulting in a surface with increased density and size of glucan exposure sites. (A) Glucan exposure density (including all singlet glucan and multiglucan exposures) increased in yeast after drug-induced glucan unmasking. Glucan exposure density was also significantly greater in untreated hyphae than in untreated yeast. (B) The drug-induced unmasking caused a significant size increase for multiglucan exposures in yeasts. Untreated hyphal cell walls also exhibited larger multiglucan exposures than untreated yeasts. (C) The number of localizations per multiglucan exposure was not significantly altered by drug-induced unmasking in yeast or hyphae, but untreated hyphae displayed a moderately greater number of localizations per multiglucan exposure than untreated yeasts. *$p < 0.01$.

so Ripley's *K* statistics for experimental and simulated data were comparable because they included identical edge effects. We observed no significant nonrandomness in glucan localization at any length scale from 10 to 1000 nm for any of the conditions tested. We note that Ripley's *K* statistic is an ensemble measurement of local spatial structure, so this statistic will provide a measurement of structure that reflects the tendency in the majority of the data (i.e., singlet glucan exposures). Ripley's *K* statistic may not be sufficiently sensitive to detect the small minority population of multiglucan exposures or changes in multiglucan exposures against a background of the majority singlet glucan exposures. Our findings suggest that there is no long-range structure to glucan exposure beyond the singlet glucan and multiglucan exposures described here.

DISCUSSION

β-(1,3)-Glucan is found commonly in the fungal phyla Zygomycota, Basidiomycota, and Ascomycota (of which *C. albicans* is a member; Ruiz-Herrera and Ortiz-Castellanos, 2010). It is a highly immunogenic molecular pattern associated with activation of dendritic cells, macrophages, and neutrophils, primarily via Dectin-1, but also recognized by β_2-integrin. Exposure of these receptors to β-glucan is an important determinant of innate immune host defense activation. Indeed, the concept of β-glucan masking by other cell-wall moieties has been invoked for several pathogenic fungal species (e.g., *C. albicans*, *Histoplasma capsulatum*, and *Aspergillus fumigatus*) as a mechanism for fungal control of β-glucan exposure (Gantner *et al.*, 2005; Wheeler and Fink, 2006; Wheeler *et al.*, 2008; Rappleye *et al.*, 2007; Edwards *et al.*, 2011; Carrion *et al.*, 2013; Shepardson *et al.*, 2013). Therefore masking of β-glucan represents a potentially important and common mechanism of immune evasion used by pathogenic fungi.

The physical mechanism of β-glucan masking in *C. albicans* is believed to involve covering of deeper β-glucan layers with superimposed mannoproteins that are abundant in the outer surface of the cell wall (Wheeler and Fink, 2006). Of interest, members of the Als family, which are large N- and O-mannosylated proteins anchored in the cell wall, have been shown to rearrange to form amyloid aggregates that are implicated in cell–cell and cell–surface adhesion, as well as biofilm formation (Garcia *et al.*, 2011). Mechanical stimulation of Als5p triggers a switch from a random distribution in the cell wall to a clustered, amyloid distribution on the time scale of tens of minutes (Alsteens *et al.*, 2010; Chan and Lipke, 2014). This lateral rearrangement of Als-family mannoproteins could provide a mechanistic basis for unmasking of β-glucan. In addition, cell-wall damage and dysfunctional glycan biogenesis activate the mitogen-activated protein kinase Cek1p-mediated cell-wall salvage pathway, inducing genes related to protein mannosylation (Ernst and Pla, 2011). *C. albicans cek1* deletion mutants exhibit increased β-glucan exposure and Dectin-1 mediated responses by DCs and macrophages (Galán-Díez *et al.*, 2010). This suggests that Cek1p signaling could be involved in maintaining a mannoprotein-based layer that masks β-glucan.

Previous optical investigations of β-glucan exposure used methods with diffraction-limited resolution. Although these methods can assess total exposure, they are not able to accurately measure β-glucan exposure geometry or structural changes that might accompany unmasking. Our superresolution imaging approach provides a view of *C. albicans* cell-wall β-glucan exposure at an unprecedented level of detail. An important caveat is that our specimens were fixed because probe mobility would degrade the accuracy of dSTORM measurements. It is conceivable that fixation might alter cell-wall structure and β-glucan exposure geometry. However, our comparisons of β-glucan exposure by confocal microscopy on live, fixed, and ultraviolet (UV)-killed *C. albicans* yeast demonstrate that, at least at the level of bulk β-glucan exposure, fixed yeasts exhibit glucan exposure that is more similar to live cells than UV-killed yeasts (Supplemental Figure S4). This suggests that our fixation approach has minimal effect on β-glucan exposure. In addition, it is unlikely that any minor effects of fixation on β-glucan nanostructure would affect relative changes in β-glucan exposure (e.g., ±caspofungin) such as we examined.

Overcounting of labeled molecules in dSTORM data sets contributes an artificial clustering at length scales corresponding to the precision of dSTORM localization. This phenomenon can also artificially inflate the size of true structures and renders quantitative comparisons of dSTORM observations difficult. Therefore methods to limit or eliminate dSTORM probe overcounting are of considerable interest to the field of superresolved fluorescence imaging. Existing solutions to this challenge are scarce. One previously reported approach to address overcounting in dSTORM data sets is pair correlation (Veatch *et al.*, 2012). The sparseness of localizations in our data

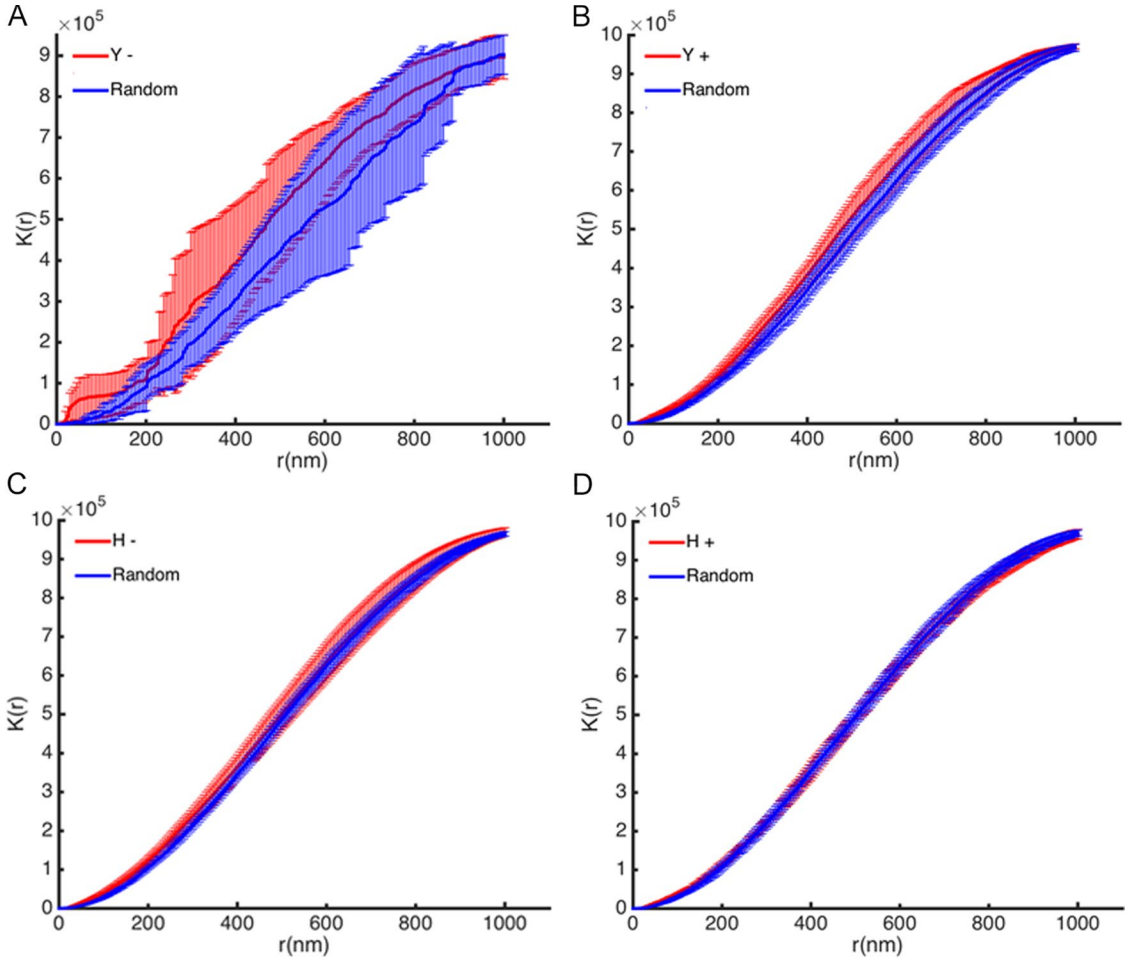

FIGURE 9: Ripley's *K* function statistical analysis indicates that there is no long-range nonrandomness in glucan exposure spatial distribution. (A–D) The Ripley *K* values of untreated yeasts were plotted against *K*(*r*) of an equivalent localization density random distribution generated for each experimental region of interest analyzed. The glucan exposure resembles a random spatial organization at length scales measured (10–1000 nm).

sets, coupled with the fact that multiglucan exposures are minority features of β-glucan exposure patterns, creates difficulty in using this ensemble method because spatial correlation methods operate best on highly multiply labeled structures, where there are numerous data points to correlate. In addition, the pair correlation method is designed to detect features with a specified spatial distribution of probes (i.e., Gaussian distribution), but this distribution is not known a priori in our case. Further, during the preparation of this article, a novel Voronoï-based segmentation method was reported that could provide a means of partially reducing dSTORM multiple localizations, but the application of this novel method to β-glucan exposure dSTORM data sets requires further investigation (Levet *et al*., 2015). We developed the H-SET to minimize the effect of overcounting in dSTORM data from sparsely labeled glucan exposures on fungal cell walls. Figure 6 indicates that, in simulated dSTORM data, we could consistently and robustly collapse multiply observed dSTORM probes to recover accurate probe localizations at domain density of 10^{-6}–10^{-5}/nm^2. Furthermore, Figure 7 indicates that, in experimental dSTORM data sets, we were able to collapse multiply observed glucan probe signals into localizations. The characteristics of such collapses indicated that the H-SET algorithm performed similarly across the range of sample conditions tested. Finally, H-SET performed similarly in collapsing multiple observations in dSTORM datasets from cell walls and from known single probes sparely distributed on glass. These findings give us confidence that the H-SET algorithm provides β-glucan exposure localization data that can reliably be analyzed by various clustering algorithms (i.e., DBSCAN) to investigate nanoscale β-glucan exposure geometry with minimal influence of overcounting of dSTORM probes.

An interpretation of the mechanism of β-glucan masking described here would most likely predict that an increase in β-glucan exposure size accompanies unmasking of β-glucan on *C. albicans*. We observed increased β-glucan staining by confocal imaging and increased phagocytic response by DCs for caspofungin-treated *C. albicans* yeasts, and these have previously been considered hallmarks of β-glucan unmasking. Strikingly, the *C. albicans* cell wall displays predominantly singlet-glucan exposures in all conditions tested, suggesting that most glucan exposures are likely to be single receptor binding sites. In *C. albicans* yeast, multiglucan exposures increased in nanoscale dimension during caspofungin-induced unmasking. Yeast also regulated overall glucan exposure levels by increasing the density of these unitary exposures upon drug-mediated unmasking. The fold change in density of β-glucan exposures observed in treated versus untreated yeast was comparable to that observed by confocal imaging.

The increased total β-glucan exposure observed in confocal fluorescence images of drug-treated hyphae (Figure 1) was not reflected in our analysis of nanoscale hyphal glucan exposure geometry. We

believe that this is due to the fact that we could not accurately perform dSTORM measurements on hyphal tips, which is where the majority of the drug-induced unmasking seems to occur. Hyphae normally attach to and grow along surfaces horizontally, so most hyphal tips can only be imaged in cross section, not *en face*. We did not perform dSTORM analysis on cross-sectional images of hyphal tips, to avoid distortion of glucan exposure geometries, as addressed in Figure 3. The few hyphal tips that could be imaged in a more *en face* orientation were poorly anchored to the substrate, and the dSTORM data displayed unacceptably high localization error, most likely stemming from sample motion during dSTORM acquisition. Hyphal tips were imaged for confocal quantification of β-glucan exposure, so the increase in β-glucan exposure at these sites was quantified in these data. However, our inability to image hyphal tips by dSTORM provides the most likely explanation for the lack of nanoscale changes to β-glucan exposure on hyphal lateral cell walls.

Our data support a model of β-glucan unmasking in which glucan exposure/Dectin-1 binding sites increase in density (exposure sites per surface area) and the size of individual exposure sites increases (Figure 10). These nanoscale changes in β-glucan exposure geometry are potentially significant for induction of Dectin-1 signaling. The Dectin-1 cytoplasmic tail contains a hemITAM motif, which is believed to require dimerization to efficiently recruit and activate Syk. Therefore the local density of Dectin-1 binding sites, particularly in multiglucan exposures, could control the extent of Dectin-1 dimerization and hemITAM activation. Previous studies with glucan-coated beads suggested that these beads must be >200 nm in diameter to be stimulatory for ROS burst (Goodridge *et al.*, 2011). We did not observe the appearance of glucan exposure structures at the >200-nm length scale (Figure 8B), even after caspofungin-induced unmasking of β-glucan. However, the directly relevant dimension is not the diameter of the bead but the size of the interface between the bead and a leukocyte plasma membrane, and this interface might be considerably smaller than the bead. Further studies will be required to rigorously test the effect of nanoscale β-glucan presentation geometry on Dectin-1 activation, and our results provide a foundation for such studies. Furthermore, increasing binding avidity is a common theme in immunoreceptor C-type lectin biology due to the typically low affinity of interaction between a single receptor's binding domain and its target glycan. For instance, the C-type lectin DC-SIGN attains high-avidity binding of fungal mannan through constitutive tetramerization and higher-order assembly into membrane nanodomains. Dectin-1 possesses a single carbohydrate domain per polypeptide, and, unlike DC-SIGN, it is not known to be constitutively oligomeric. Therefore regulation of ligand density in nanoscale glucan exposure sites could be an important factor in creating a sufficiently high local membrane density of Dectin-1 to support signaling.

MATERIALS AND METHODS

Yeast sample preparation

C. albicans SC5314 (ATCC, Manassas, VA) was grown in Difco yeast extract/peptone/dextrose (YPD broth medium [242820; BD Bioscience, San Jose, CA]) at 30°C overnight. Yeast cells were harvested by centrifugation, washed three times with phosphate-buffered saline (PBS), and plated sparsely on ethanol-washed coverslips (~10^5 cells/coverslip) within wells of a six-well plate. Cells were then allowed to adhere to coverslips by growth in fresh YPD at 30°C (for yeast) or RPMI medium 1640 (21870; Life Technologies, Grand Island, NY) at 37°C (for hyphae) for 1 h. These growth conditions resulted in adherent yeast or hyphae, respectively. After 1 h of growth, the coverslip was washed twice with PBS to remove any remaining nonadherent cells. Then fresh medium with caspofungin was added (YPD + caspofungin [100 ng/ml; SML0425; Sigma-Aldrich, St. Louis, MO] for yeast or RPMI + caspofungin for hyphae), and cells were cultured for an additional 4 h at 30°C (for yeast) or 37°C (for hyphae). For untreated controls, the same procedure was applied with the omission of caspofungin. The cells were fixed with fresh made 4% paraformaldehyde (PFA) for 15 min, followed by three washes of PBS. For heat-killed yeast, 10^8/ml yeasts were heated at 56°C for 30 min. For UV-killed yeast, 10^6/ml yeasts were exposed to UV light at 120,000 μJ/cm^2 for 3 min (Stratalinker 2400; Stratagene, La Jolla, CA).

Dendritic cells

Human peripheral blood mononuclear cells (PBMCs) were obtained from discarded leukocyte reduction filter effluent (United Blood Services, Albuquerque, NM). To recover cells from leukocyte reduction filters, those filters were back-flushed with 300 ml of Hanks' balanced salt solution using a peristaltic pump (155 rpm; Watson-Marlow, Falmouth, United Kingdom). The collected cells from either donor were spun over Ficoll-Paque Plus (17-1440-03; GE Healthcare Bio-Science, Pittsburgh, PA) to isolate PMBCs. Monocytes were purified by adherence on tissue culture flasks. Immature dendritic cells were prepared by differentiation of monocytes in RPMI supplemented with 10% fetal bovine serum, 1% penicillin/streptomycin, 10 mM 4-(2-hydroxyethyl)-1-piperazineethanesulfonic acid, 1 mM sodium pyruvate, 500 IU/ml human interleukin-4 (200-04; Peprotech, Rocky Hill, NJ), and 800 IU/ml human granulocyte macrophage colony–stimulating factor (Leukine, Bayer Healthcare Pharmaceuticals, Seattle, WA) at 37°C and 5% CO_2 for 7 d. This use of human blood products was reviewed and approved by the University of New Mexico Health Sciences Center Human Research Review Committee.

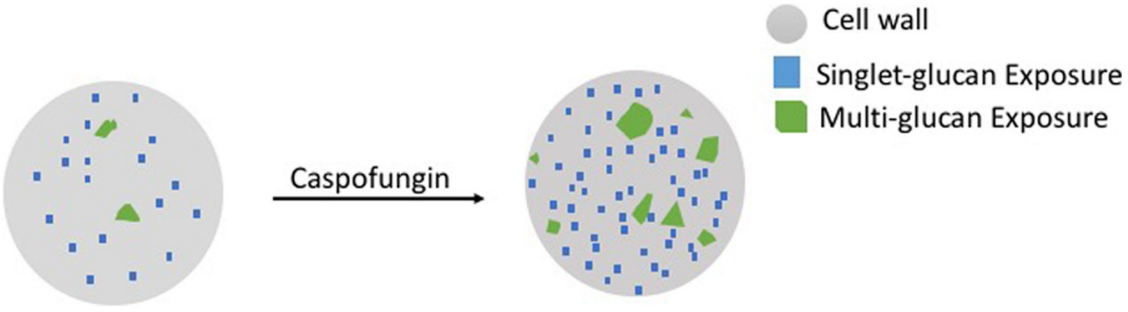

FIGURE 10: Proposed caspofungin-induced cell wall spatial remodeling. The majority of glucan exposure sites on yeast cell walls are glucan singlet exposures. Caspofungin treatment alters the nanoscale geometry of glucan exposure. Drug-unmasked yeasts present a cell-wall surface with increased total glucan exposure due to a higher density of singlet glucan and multiglucan exposures, as well as larger multiglucan exposures.

Phagocytosis assay

Fixed untreated or caspofungin-treated yeasts were stained with Calcofluor White (F3543; Sigma-Aldrich) at a concentration of 25 μg/ml for 20 min at 25°C. Then the yeasts were biotinylated with Biotin-NHS (H1759; Sigma-Aldrich) at a concentration of 50 μM for 1 h at 25°C in PBS at pH 8.5. After staining, these yeast particles were added to live DC cultures for 1 h. After the first 45 min of this 1-h staining period, 50 μM streptavidin–Alexa Fluor 647 (AF647) in RPMI warmed to 37°C was added to the live DC culture for 15 min. At this point the DCs were fixed with 4% PFA in PBS for 10 min at 25°C, followed by extensive PBS washing.

Fixed yeast particles were imaged with a FV1000 laser scanning confocal microscope (Olympus, Center Valley, PA). Calcofluor White (marker for all yeast) was excited with a 50- mW, 405-nm diode laser operated at 1% power, and streptavidin-conjugated Alexa Fluor 647 (marker for only external yeast) was excited with a 20-mW, 635-nm diode laser operated at 1% power.

Bound and internalized yeast were enumerated manually on a per-DC basis in all 3D confocal data sets. Bound yeasts were identified based on their location on DCs (differential interference contrast [DIC]) and positive signal for both Calcofluor White and AF647 emission. Internalized yeasts were identified by apparent localization inside a DC (DIC) emission in the Calcofluor White channel only. We calculated the percentage of DCs internalizing one or more yeast and the phagocytosis index (PI) for each DC. PI was calculated as the number of yeasts that were identified internalized divided by the total number of yeasts associated with the same DC (i.e., surface-bound plus internalized yeasts).

Confocal fluorescence imaging

C. albicans β-glucans were sequentially labeled with β-(1,3)-D-glucan antibody (10 μg/ml, 400-2; Biosupplies Australia, Bundoora, Australia) and Alexa Fluor 488 goat anti-mouse immunoglobulin G (2 μg/ml, A11029; Invitrogen, Grand Island, NY) in PBS for 30 min at room temperature for both antibodies. Yeast samples were imaged in PBS mounted in an Attofluor Cell Chamber (A7816; Life Technologies) with an FV 1000 laser scanning confocal microscope (Olympus) equipped with a 60×/1.42 numerical aperture (NA), PlanApochromat oil immersion objective. Alexa Fluor 488 was excited with a 473-nm laser operated at 1% power. These lines were reflected to the specimen by a 405/473/559/635 multiedge main dichroic element, and emission was routed through the main dichroic mirror and confocal pinhole (115-nm diameter) to secondary longpass dichroics (or a mirror), followed by bandpass emission filters in front of independent photomultiplier detectors.

Confocal image analysis was carried out by a custom program written in MATLAB (MathWorks, Natick, MA) that was modified from previous code provided by Adam Hoppe (Department of Chemistry, South Dakota State University, Brookings, SD). In general, background intensity was calculated as the average intensity of a selected cell-free region of each image. After subtracting background signal, the average intensity of yeast was obtained by the summed intensity of yeast cells (hand-selected ROI) divided by the area of the ROI.

Simulation of projection distortion in superresolution images of fungal cell walls

Simulations were performed using a custom MATLAB program. Two-dimensional projections of domains lying on latitude-bounded sectors of the surface of a sphere of radius 2500 nm were simulated. This was done by first generating 2D Gaussian domains in a rectangular region of equivalent area to the desired spherical sector with user-defined values for domain density, sigma (variance), and minimum domain-center separation. The actual number of domains produced was determined from a Poisson distribution that depended linearly on the domain density; this number could be reduced, however, when enforcing the domain-center separation constraint. The domains were then projected onto the spherical surface between specified latitude (ϕ) lines and finally projected onto the equatorial 2D plane. The size of a simulated domain was characterized by its convex hull and the area within, expressed as the diameter of the circle of equivalent area. Each study was averaged over 100 simulations.

Superresolution imaging

Alexa Fluor 647 NHS Ester (succinimidyl ester) (A20006; Invitrogen) was used to label soluble recombinant human Dectin-1 (1859DC; R&D Systems, Minneapolis, MN) following the manufacturer's labeling protocol. Briefly, Alexa Fluor 647-SE and Dectin-1 were mixed at 5:1 M ratio in PBS (pH 8, adjusted by 1.0 M $NaHCO_3$). The reaction was carried out overnight at 4°C in the dark. The labeled proteins were purified by Zeba Spin Desalting Column (7-kDa MWCO, 89882; Thermo Scientific, Waltham, MA). The average degree of labeling was one to two fluorophores per protein as determined by absorption spectroscopy. Fungal cells were labeled with the Dectin-1-AF647 probe at 1 μg/ml for 30 min at room temperature, and excess probe was washed off with PBS for at least three times before dSTORM imaging.

Fixed yeast cells were imaged in a buffer containing 50 mM Tris, 10% (wt/vol) glucose, 10 mM NaCl, 40 μg/ml catalase (C40; Sigma-Aldrich), 500 μg/ml glucose oxidase (G0543; Sigma-Aldrich), and 10 mM cysteamine (M9768; Sigma-Aldrich), pH 8.0. Data were recorded on an Olympus IX-71 microscope equipped with an objective-based TIRF illuminator using an oil-immersion objective (PlanApo N, 150×/1.45 NA; Olympus) in an oblique illumination configuration (illumination at a subcritical angle). The sample was excited with a 637-nm laser (laser diode, HL63133DG; Thorlabs, Newton, NJ) with custom-built collimation optics. The samples were excited at low intensity (0.03 kW/cm^2) in order to find a region of interest. The excitation intensity was then increased to ~1 kW/cm^2 for dSTORM imaging. The fluorescence filter setup consisted of a dichroic mirror (650 nm; Semrock, Rochester, NY) and an emission filter (692/40; Semrock). Image movies were recorded with an electron-multiplying charge-coupled device camera (iXon 897; Andor, Belfast, United Kingdom) using an exposure time of 20 ms with electron multiplication gain 200 (Smith *et al.*, 2010; Nieuwenhuizen *et al.*, 2013).

Superresolution image reconstruction

dSTORM image reconstruction was carried out by estimating the emitter positions using a fast, maximum likelihood–based algorithm to localize single emitters. This robust algorithm allowed rapid and efficient localization of single-molecule events (Smith *et al.*, 2010; Huang *et al.*, 2011). Fits were accepted if the fit precisions, given by the square root of Cramér–Rao lower bound (CRLB), were <11 nm (Smith *et al.*, 2010) and the data in the fitting regions were consistent with a single-emitter model at a 0.01 level of significance (Huang *et al.*, 2011). Fits separated by less than four time frames were grouped together with an improved position estimate and fit precision.

Hierarchical single-emitter hypothesis test

We developed a top-down hierarchical clustering algorithm in MATLAB to collapse clusters of observations (precollapsed point) of blinking fluorophores into a single estimate of the true location of the fluorophore. For a cluster of observations to be collapsed into a single fluorophore position, we make a hypothesis test with the null hypothesis that all observations come from the same fluorophore.

The null hypothesis is not rejected if the p value is larger than a specified level of significance. The p value is calculated using the log-likelihood ratio statistic, R, which is calculated as $R = -2\log(L/L_0)$, where L is the likelihood of the N observations, given a fluorophore located at the maximum likelihood position and given the observation uncertainties, and L_0 is the likelihood of the N positions, assuming there are N independent fluorophores. In M dimensions, R is chi-squared distributed with $M(N-1)$ degrees of freedom. For our analysis here, $M = 2$.

The maximum likelihood estimate of the collapsed position is the variance-weighted mean value of the observed positions:

$$\bar{X} = \frac{\sum_{i}^{N}=1 \frac{X_i}{(\sigma_i')^2}}{\sum_{i}^{N}=1 \frac{1}{(\sigma_i')^2}} \quad (1)$$

where

$$(\sigma_i') = \sigma_i^2 + \sigma_{\text{reg}}^2 \quad (2)$$

Here X_i and σ_i are the observed positions of the fluorophores and the uncertainties in the observed positions, respectively; σ_{reg} is the registration error (zero in our analysis because of the short intervals between frames), and σ_i is the modified uncertainty including the effects of drift correction.

The uncertainty in the position of the collapsed fluorophore is then calculated from the variance of the weighted mean:

$$\bar{\sigma}^2 = \frac{1}{\sum_{i=1}^{N} \frac{1}{(\sigma_i')^2}} \quad (3)$$

The algorithm proceeds in two passes. The first uses the MATLAB standard hierarchical clustering algorithm (linkage) to create a binary tree of relationships connecting observations together in clusters of varying sizes (Figure 5). Each node of the tree corresponds to a cluster of one or more observations. That is, each node splits into two branches, which end at either a single observation or a node representing a smaller cluster of observations. The algorithm starts at the top node, which collects together all of the observations (the tree grows downward) and checks whether this cluster of observations could be due to a point source according to the level of significance (LoS) assigned by the user (the default is LoS = 0.01). If yes ($p >$ LoS), the cluster is collapsed into a single localization (postcollapse point), and the algorithm terminates at this node. If no ($p \leq$ LoS), the two branches are traversed in turn, making the same check on the nodes at the ends. Any time the test succeeds, all of the observations represented by that node are collapsed into a single localization, and the algorithm does not descend further.

The final output is the set of localizations discovered, which may be collapsed clusters of observations or isolated observations that were not collected into any larger cluster by the algorithm. We chose to traverse the linkage tree top-down, as 1) the significance test works better for larger clusters, and 2) bottom-up traversal could produce different results depending on which points were collapsed first, that is, on the order of collapsing.

In rare instances, observations that should be collapsed together with other observations are not included in the same hierarchical node and are missed. Therefore our algorithm proceeds to a second pass of clustering to minimize multiple counting of probes in these instances. The second pass of the algorithm uses a user-specified clustering algorithm such as hierarchical, DBSCAN, Getis based, and so on to cluster the localizations together produced by the first pass (Ester *et al.*, 1996; Daszykowski *et al.*, 2001; Itano *et al.*, 2014). In our application of H-SET, we used the DBSCAN algorithm in the second pass. H-SET checks each cluster it finds in turn with the foregoing significance test and collapses any cluster that passes (i.e., a cluster deemed to be due to a point source localization). Most of the collapsing is typically done by the first pass; the second pass sometimes finds a few more small clusters to collapse.

As noted, the DBSCAN was used to identify multiglucan exposure structures on cell walls. The value of ε, which determines the search radius for localization clustering, was set to 50 nm (Daszykowski *et al.*, 2001). A minimum of three localizations was used to define a multiglucan exposure. To clearly distinguish different subsets of glucan exposure, we have defined postcollapse single point glucan exposure as singlet-glucan exposure, postcollapsed clusters with three or more points as multiglucan exposure, and any singlet or multiexposure as glucan exposure.

Statistical spatial analysis of dSTORM data with Ripley's *K* function

Analysis with Ripley's *K* function was implemented based on previously published code for analysis of immunogold images (http://stmc.health.unm.edu/tools-and-data/index.html; Zhang *et al.*, 2006). Simulated random distributions of points of equivalent density to data sets in 1 μm × 1 μm regions were generated with custom MATLAB code and analyzed by the same Ripley's *K* function software. Comparison with random point distributions with the same density and region geometry as the data sets controlled for the edge effects on $K(r)$.

Statistics

Box plots were used to display most of the data due to their ability to depict summary statistics and population distributions for the measured parameters. These box plots show a median (solid line) within a box representing the interquartile range (IQR; 25th to 75th percentile of the population). The whiskers below and above the IQR box represent the 1st and 99th percentiles of the data set. Crosses are used to depict data points that fell outside of these latter percentiles. Statistical comparisons generally used the Mann–Whitney *U* test implemented using standard MATLAB functions with the exception of Ripley's *K* analysis, in which random simulations and dSTORM data sets were compared by Student's *t* test.

Computer code

Software created for data analysis and simulation is accessible at http://stmc.health.unm.edu/tools-and-data/index.html.

ACKNOWLEDGMENTS

We gratefully acknowledge technical advice from Carolyn Pehlke, Chris Valley, Sam Schwartz, Sheng Liu, and Stanly L. Steinberg and critical review of the manuscript by Jan Oliver. This research was supported by the University of New Mexico Center for Spatiotemporal Modeling of Cell Signaling (National Institutes of Health 5P50GM085273), a New Mexico Medical Trust Fund UNM SOM RAC award (A.K.N.), the New Mexico Cancer Nanotechnology Training Center (CA-R25153825; M.S.G.) and National Institutes of Health Grant R01AI116894 (A.K.N.). We acknowledge support from the University of New Mexico Cancer Center's Bioinformatics and High-Dimensional Data Analysis Shared Resource (National Institutes of Health/National Cancer Institute P30CA118100) and University of New Mexico Center for Advanced Research Computing.

REFERENCES

Adams EL, Rice PJ, Graves B, Ensley HE, Yu H, Brown GD, Gordon S, Monteiro MA, Papp-Szabo E, Lowman DW, *et al.* (2008). Differential high-affinity interaction of dectin-1 with natural or synthetic glucans is dependent upon primary structure and is influenced by polymer chain length and side-chain branching. J Pharmacol Exp Ther 325, 115–123.

Alsteens D, Garcia MC, Lipke PN, Dufrêne YF (2010). Force-induced formation and propagation of adhesion nanodomains in living fungal cells. Proc Natl Acad Sci USA 107, 20744–20749.

Anderson DJ, Kirkland KB, Kaye KS, Thacker PA, Kanafani ZA, Auten G, Sexton DJ (2007). Underresourced hospital infection control and prevention programs: penny wise, pound foolish. Infect Control Hosp Epidemiol 28, 767–773.

Banchereau J, Steinman RM (1998). Dendritic cells and the control of immunity. Nature 392, 245–252.

Bizerra FC, Melo AS, Katchburian E, Freymüller E, Straus AH, Takahashi HK, Colombo AL (2011). Changes in cell wall synthesis and ultrastructure during paradoxical growth effect of caspofungin on four different Candida species. Antimicrob Agents Chemother 55, 302–310.

Brown GD, Herre J, Williams DL, Willment JA, Marshall ASJ, Gordon S (2003). Dectin-1 mediates the biological effects of beta-glucans. J Exp Med 197, 1119–1124.

Brown GD, Taylor PR, Reid DM, Willment JA, Williams DL, Martinez-Pomares L, Wong SYC, Gordon S (2002). Dectin-1 is a major beta-glucan receptor on macrophages. J Exp Med 196, 407–412.

Brown J, O'Callaghan CA, Marshall ASJ, Gilbert RJC, Siebold C, Gordon S, Brown GD, Jones EY (2007). Structure of the fungal β-glucan-binding immune receptor dectin-1: Implications for function. Protein Sci 16, 1042–1052.

Carrion SDJ, Leal SM, Ghannoum MA, Aimanianda V, Latgé J-P, Pearlman E (2013). The RodA hydrophobin on Aspergillus fumigatus spores masks dectin-1- and dectin-2-dependent responses and enhances fungal survival in vivo. J Immunol 191, 2581–2588.

Chan CXJ, Lipke PN (2014). Role of force-sensitive amyloid-like interactions in fungal catch-bonding and biofilms. Eukaryot Cell 13, 1136–1142.

Cheng S-C, Joosten LAB, Kullberg B-J, Netea MG (2012). Interplay between Candida albicans and the mammalian innate host defense. Infect Immun 80, 1304–1313.

Daszykowski M, Walczak B, Massart DL (2001). Looking for natural patterns in data. Part 1. Density-based approach. Chemometrics Intelligent Lab Syst 56, 83–92.

Davies JM, Stacey AJ, Gilligan CA (1999). Candida albicans hyphal invasion: thigmotropism or chemotropism. FEMS Microbiol Lett 171, 245–249.

Edwards JA, Alore EA, Rappleye CA (2011). The yeast-phase virulence requirement for α-glucan synthase differs among Histoplasma capsulatum chemotypes. Eukaryot Cell 10, 87–97.

El-Kirat-Chatel S, Beaussart A, Alsteens D, Jackson DN, Lipke PN, Dufrêne YF (2013). Nanoscale analysis of caspofungin-induced cell surface remodelling in Candida albicans. Nanoscale 5, 1105–1115.

Ernst JF, Pla J (2011). Signaling the glycoshield: maintenance of the Candida albicans cell wall. Int J Med Microbiol 301, 378–383.

Ester M, Kriegel H, Sander J, Xu X (1996). A density-based algorithm for discovering clusters in large spatial databases with noise. Proceedings of the Second International Conference on Knowledge Discovery and Data Mining (KDD-96), Palo Alto, CA: AAAI Press, 226–231.

Galán-Díez M, Arana DM, Serrano-Gómez D, Kremer L, Casasnovas JM, Ortega M, Cuesta-Domínguez A, Corbí AL, Pla J, Fernández-Ruiz E (2010). Candida albicans beta-glucan exposure is controlled by the fungal CEK1-mediated mitogen-activated protein kinase pathway that modulates immune responses triggered through dectin-1. Infect Immun 78, 1426–1436.

Gantner BN, Simmons RM, Underhill DM (2005). Dectin-1 mediates macrophage recognition of Candida albicans yeast but not filaments. EMBO J 24, 1277–1286.

Garcia MC, Lee JT, Ramsook CB, Alsteens D, Dufrêne YF, Lipke PN (2011). A role for amyloid in cell aggregation and biofilm formation. PLoS One 6, e17632.

Goodridge HS, Reyes CN, Becker CA, Katsumoto TR, Ma J, Wolf AJ, Bose N, Chan ASH, Magee AS, Danielson ME, *et al.* (2011). Activation of the innate immune receptor Dectin-1 upon formation of a phagocytic synapse. Nature 472, 471–475.

Griffié J, Boelen L, Burn G, Cope AP, Owen DM (2015). Topographic prominence as a method for cluster identification in single-molecule localisation data. J Biophotonics 8, 925–934.

Grubb SEW, Murdoch C, Sudbery PE, Saville SP, Lopez-Ribot JL, Thornhill MH (2008). Candida albicans-endothelial cell interactions: a key step in the pathogenesis of systemic candidiasis. Infect Immun 76, 4370–4377.

Huang F, Schwartz SL, Byars JM, Lidke KA (2011). Simultaneous multiple-emitter fitting for single molecule super-resolution imaging. Biomed Opt Express 2, 1377–1393.

Itano MS, Graus MS, Pehlke C, Wester MJ, Liu P, Lidke KA, Thompson NL, Jacobson K, Neumann AK (2014). Super-resolution imaging of C-type lectin spatial rearrangement within the dendritic cell plasma membrane at fungal microbe contact sites. Front Phys 2, 1–17.

Jain AK, Dubes RC (1988). Algorithms for Clustering Data, Upper Saddle River, NJ: Prentice-Hall.

Keating G, Figgitt D (2003). Caspofungin: a review of its use in oesophageal candidiasis, invasive candidiasis and invasive aspergillosis. Drugs 63, 2235–2263.

Lamaris GA, Lewis RE, Chamilos G, May GS, Safdar A, Walsh TJ, Raad II, Kontoyiannis DP (2008). Caspofungin-mediated beta-glucan unmasking and enhancement of human polymorphonuclear neutrophil activity against Aspergillus and non-Aspergillus hyphae. J Infect Dis 198, 186–192.

Levet F, Hosy E, Kechkar A, Butler C, Beghin A, Choquet D, Sibarita J (2015). SR-Tesseler: a method to segment and quantify localization-based super-resolution microscopy data. Nat Methods 12, 1065–1071.

Lo H-J, Köhler JR, DiDomenico B, Loebenberg D, Cacciapuoti A, Fink GR (1997). Nonfilamentous C. albicans mutants are avirulent. Cell 90, 939–949.

Mccormack PL, Perry CM, Deresinski SC (2005). A review of its use in the treatment of fungal infections. Drugs 65, 2049–2068.

Murad AMA, Leng P, Straffon M, Wishart J, Macaskill S, MacCallum D, Schnell N, Talibi D, Marechal D, Tekaia F, *et al.* (2001). NRG1 represses yeast-hypha morphogenesis and hypha-specific gene expression in Candida albicans. EMBO J 20, 4742–4752.

Nieuwenhuizen RPJ, Lidke KA, Bates M, Puig DL, Grünwald D, Stallinga S, Rieger B (2013). Measuring image resolution in optical nanoscopy. Nat Methods 10, 557–562.

Ord JK, Getis A (1995). Local spatial autocorrelation statistics: distributional issues and an application. Geogr Anal 27, 286–306.

Rappleye CA, Eissenberg LG, Goldman WE (2007). Histoplasma capsulatum alpha-(1,3)-glucan blocks innate immune recognition by the beta-glucan receptor. Proc Natl Acad Sci USA 104, 1366–1370.

Rogers NC, Slack EC, Edwards AD, Nolte MA, Schulz O, Schweighoffer E, Williams DL, Gordon S, Tybulewicz VL, Brown GD, Reis e Sousa C (2005). Syk-dependent cytokine induction by dectin-1 reveals a novel pattern recognition pathway for C type lectins. Immunity 22, 507–517.

Rubin-Delanchy P, Burn GL, Griffié J, Williamson DJ, Heard NA, Cope AP, Owen DM (2015). Bayesian cluster identification in single-molecule localization microscopy data. Nat Methods 12, 1072–1076.

Ruiz-Herrera J, Ortiz-Castellanos L (2010). Analysis of the phylogenetic relationships and evolution of the cell walls from yeasts and fungi. FEMS Yeast Res 10, 225–243.

Sengupta P, Jovanovic-Talisman T, Lippincott-Schwartz J (2013). Quantifying spatial organization in point-localization superresolution images using pair correlation analysis. Nat Protoc 8, 345–354.

Shepardson KM, Ngo LY, Aimanianda V, Latgé J-P, Barker BM, Blosser SJ, Iwakura Y, Hohl TM, Cramer RA (2013). Hypoxia enhances innate immune activation to Aspergillus fumigatus through cell wall modulation. Microbes Infect 15, 259–269.

Smith CS, Joseph N, Rieger B, Lidke KA (2010). Fast, single-molecule localization that achieves theoretically minimum uncertainty. Nat Methods 7, 373–375.

van de Linde S, Löschberger A, Klein T, Heidbreder M, Wolter S, Heilemann M, Sauer M (2011). Direct stochastic optical reconstruction microscopy with standard fluorescent probes. Nat Protoc 6, 991–1009.

Veatch SL, Machta BB, Shelby SA, Chiang EN, Holowka DA, Baird BA (2012). Correlation functions quantify super-resolution images and estimate apparent clustering due to over-counting. PLoS One 7, e31457.

Wenzel RP, Edmond MB (2001). The impact of hospital-acquired bloodstream infections. Emerg Infect Dis 7, 174–177.

Wheeler RT, Fink GR (2006). A drug-sensitive genetic network masks fungi from the immune system. PLoS Pathog 2, e35.

Wheeler RT, Kombe D, Agarwala SD, Fink GR (2008). Dynamic, morphotype-specific Candida albicans beta-glucan exposure during infection and drug treatment. PLoS Pathog 4, e1000227.

Zhang J, Leiderman K, Pfeiffer JR, Wilson BS, Oliver JM, Steinberg SL (2006). Characterizing the topography of membrane receptors and signaling molecules from spatial patterns obtained using nanometer-scale electron-dense probes and electron microscopy. Micron 37, 14–34.